

Article

Emergences of New Technology for Ultrafast Automated Mineral Phase Identification and Quantitative Analysis Using the CORIOSITY Laser-Induced Breakdown Spectroscopy (LIBS) System

Kheireddine Rifai ^{1,2,*}, Marie-Chloé Michaud Paradis ¹, Zofia Swierczek ³, François Doucet ¹, Lütffü Özcan ¹, Alejandro Fayad ³, Jing Li ³ and François Vidal ²

¹ Elemission Inc., 3410, Thimens Boulevard, Montréal, QC H4R 1V6, Canada; marie-chloe.michaud.paradis@elemission.ca (M.-C.M.P.); fdoucet@elemission.ca (F.D.); lozcan@elemission.ca (L.Ö.)

² Centre Énergie Matériaux Télécommunications, Institut National de la Recherche Scientifique, 1650 Lionel-Boulet Boulevard, Varennes, QC J3X 1S2, Canada; vidal@emt.inrs.ca

³ AXT Pty Ltd., 1/14 Brodie-Hall Drive, Bentley, WA 6102, Australia; zofia.swierczek@axt.com.au (Z.S.); alejandro.fayad@axt.com.au (A.F.); jing.li@axt.com.au (J.L.)

* Correspondence: krifai@elemission.ca; Tel.: +1-514-928-2223

Received: 11 September 2020; Accepted: 14 October 2020; Published: 16 October 2020



Abstract: Geochemical and mineralogical characterization studies play an important role in the definition of mineral deposits. Each mineral system has a unique set of minerals with different chemical makeup and physical properties. Platinum-group elements (PGEs), for example, are scarce resources with many applications. The optimization of extraction process efficiency is therefore crucial to prevent resource shortage and increased bulk prices. To improve the mineral liberation process, high throughput sensors must be added alongside the production line as part of fast process analysis implementation. Current analytical methods are either ineffective to assess PGE content, or unusable in the conditions of the processing facilities. This article shows how Laser-induced breakdown spectroscopy (LIBS) technology, developed by ELEMISSION Inc, can circumvent these drawbacks by enabling automated, ultra-fast, and precise quantitative mineral analyses in any working environment. The drill core samples that were used in this study were collected at the Stillwater platinum group element mine in the United States. The data used for the mineralogical database was validated using the TESCAN Integrated Mineral Analyzer (TIMA) instrument.

Keywords: LIBS; TIMA-X; supervised learning; drill core; PGE; automated mineralogy

1. Introduction

Platinum-group elements (PGEs) are essential for the modern economy. Platinum and palladium are well known in organic chemistry as cross-coupling catalysts for their unique coordination chemistry [1]. Recent hot topics promote an increased interest in their use as metal centers of metallodrugs [2] or metal-organic frameworks [3]. Additionally, their commercial uses as high throughput catalysts for oil fuels [4] and hydrogen evolution catalysts [5] provide green applications. PGEs are also irreplaceable constituents of many devices' data storage and electronic components such as smartphones. The demand for their use in high-technology materials, unique catalysts, and fuel evolution is ever-growing, where their applications are limited mostly by their cost.

Most PGEs occur as minor constituents of common Ni-Cu sulfide intrusions in mafic and ultramafic rocks [6]. Variations in the composition of PGE-containing intrusions make traditional analytical methods insufficient to provide in situ information on the available mineral and gangue alongside both the prospecting and extraction processes. Such in-process assessments are vital to optimize the extraction process and lower bulk price.

For scarce elements, analyzing the elemental content at the surface of drilled cores constitutes a viable prospective throughput method. The micro X-ray fluorescence spectrometry (μ -XRF) has been used to run such analyses on PGE-bearing core samples in a recent article by Meima et al. [7]. In this article, a μ -XRF probe was used combined with other sensing techniques to shorten the analysis time. Although having promising solid-state elemental analysis applications, the long dwell times do not comply with in-situ analysis goals.

Scanning electron microscopy analyzers paired with energy-dispersive X-ray spectroscopy (SEM-EDS) are commercially mature instruments rendering a mineral surface mapping. The first analyzers, called mineral liberation analyzers (MLAs), provide mineral mappings of samples and robust databases [8]. Technological improvements have been made on SEM-based analyzers, bringing on the market the Quantitative Evaluation of Materials by SCANNing electron microscopy (QEMSCAN) analyzer [9], and more recently, the TESCAN Integrated Mineral Analyzer (TIMA) [10]. To avoid surface overcharge, the cut and polished core samples or resin-embedded rock samples have to be coated with a layer of conductive carbon prior to the analysis. When the automated scanning starts, SEM-EDS instruments first generate surface maps from the count of backscattered electrons proportional to the average atomic mass of the analyzed mineral. An EDS spectrum is then generated from areas having a similar backscattered electrons (BSE) signal or following a 2D pattern, providing information on both elemental and mineral content. The mineral content analysis, based on spectral pattern recognition of the EDS spectra and applied to similar BSE signal areas, reduces the acquisition time and infer the mineralogy of the non-scanned EDS areas.

QEMSCAN and TIMA technologies both yield similar outputs. A thorough study by Honeyands et al. reported similar conclusions with both instruments, although they were not able to discriminate between hematite and magnetite minerals using the TIMA instrument [11]. That conclusion is quite specific to the chosen parameters and samples and does not affect the TIMA instrument's main high-resolution task.

The PGE-bearing core samples analyzed in the present study come from the Stillwater Complex, Montana (USA). The USGS organization recently published the Chromium and Iron Mountain areas geological survey data from the same complex. The SEM-EDS technology used for all samples was the TIMA-X generation [12]. Therefore, the reputation of the TIMA-X instrument paired with recent surveys really makes the TIMA-X instrument the ultimate choice to compare the SEM-EDS technology to other techniques.

A downside of such analysis is that the total SEM-EDS analysis duration is lengthy and requires a laborious sample preparation in a controlled laboratory environment. The SEM-EDS method is, therefore, incompatible for fast analysis. SEM-EDS based technologies are confined to laboratory applications because of their bulky nature and their requirements of special infrastructures such as vibration-free concrete slate and temperature control laboratory. These requirements make it difficult to deploy in remote locations near the exploration activities to reduce the analysis downtime. Additionally, the detectability of elements using X-ray based elemental analysis techniques depends on the emitted photons interacting with the material. Light elements emit none or low energy X-ray photons when excited. Since the EDS beam penetrates a fair distance beneath the surface, the lowest energy photons are absorbed within the sample. As a consequence, only elements with an atomic number above 11 are efficiently detectable using EDS [13]. The sensitivity of the EDS elemental analysis is also too poor to quantify trace elements (<0.001%).

Altogether, SEM-EDS methods are ubiquitous in the mining industry. No such analysis can render both the elemental content and the mineral content at comparable resolutions and industrial grade.

There are major applications for these instruments, but analysis duration and sample preparation make in-situ SEM-EDS analyses nearly impossible. Current efficiency issues are not resolved nor possibly answered just by the previously described methods. An ultrafast analyzer capable of both elemental and mineral surface imaging is still essential to make scarce PGE extraction efficient and waste-limited, as well as for other mineral mapping issues.

Laser-induced breakdown spectroscopy (LIBS) has been more and more identified as a robust all-state multi-elemental analyzer. To assess mineral liberation during process analysis, a lower spatial resolution may be enough to map the abundance of key minerals; therefore, LIBS technology is applicable to both high-resolution mapping and fast process analysis. Published LIBS studies applied to the mining industry have mainly focused on the quantitative analysis of major and minor elements (e.g., Harmon et al. (2013) [14] and Harmon et al. (2019) [15]). Jolivet et al. reviewed the recent advances and applications of LIBS imaging [16]. Gottlieb et al. introduced a clustering algorithm (EM Lustering) applied to heterogeneous building materials (concrete) to extract spectral information from non-relevant aggregates and cement matrix [17]. It was only in the last few years that LIBS began to be used to determine mineral phases from atomic emission spectra patterns. More precisely, LIBS pattern recognition algorithms consisted mainly of unsupervised machine learning methods to provide qualitative and quantitative mineral phases analysis. For instance, Romppanen et al. [18] used the singular value decomposition (SVD, a principal component analysis (PCA) kernel) for the unsupervised classification of minerals containing rare earth elements in rock samples. Maps assessing the mineralogy in the sampled area have been constructed. They demonstrated using SVD that the percentage of yttrium-bearing minerals can be calculated from fine-grained rock samples.

Recently, Pagnotta et al. proposed a quantitative micro-LIBS elemental imaging method based on the application of the self-organizing map (SOM), an unsupervised machine learning algorithm, for the determination of the different classes of materials in the samples [19]. The SOM step is followed by a calibration-free-LIBS analysis (CF-LIBS) of the average spectra. More recently, El Haddad et al. applied the Multi-Curve Resolution Alternating Least Square (MCR-ALS) algorithm to the spectral data obtained by LIBS to classify and quantify the minerals present in sectioned rock fragments [20]. In their study, the samples were first analyzed using SEM-EDS. Then, the LIBS spectral patterns identified as single-phase minerals were deconvolved using an unsupervised MCR-ALS algorithm that uses a “pure spectrum” as a seed to help the model converge. Acceptable agreement between LIBS and SEM-EDS results was reported.

Nikonow et al. proposed the combination of LIBS, micro-EDXRF, and hyperspectral infrared reflectance analysis to provide valuable information within each technique’s limitations, such as spatial resolution or elemental sensitivity [21]. The aim of the combinatory method was to lower the sample preparation and measurement duration. The data obtained using this method was combined with the supervised spectral angle mapper algorithm (SAM) to generate mineral phases imaging [21]. Additionally, Meima et al. used LIBS and a supervised pattern recognition algorithm called Spectral Angle Mapper (SAM) to identify the minerals present in two drill cores from the South African Merensky Reef mine [7]. In this work, LIBS analyses were performed using a confocal microscope (60 μm spot size) and a drill core scanner (200 μm spot size). The results were then compared to data collected using an automated SEM Mineral Liberation Analysis (SEM-MLA) instrument. The results were promising as a good match between the mineral maps generated from both analyzers was achieved. However, the authors mention that Fe sulfides (pyrite or pyrrhotite) could not be discriminated using the SAM algorithm. The acquisition time of LIBS data lasted 2–3 days [7], which is way too long for practical applications in the mining industry. In addition, the LIBS quantitative mineral content was not presented nor compared to the SEM-MLA results. The lacking of this validation step is unfortunate since mineral content is normally available using SEM-MLA.

Finally, Nardecchia et al. [22] used the k-means unsupervised pattern recognition algorithm to identify the different mineral phases. This study consisted of two steps: the main mineral phases were first identified, then the sub-phases. This approach could be useful to analyze rock specimens

exhibiting various elemental compositions in a single mineral grain. However, the convergence of the unsupervised algorithm on mixed mineral signatures might be an issue. In their study, the mineralogical classes and subclasses identified by the pattern recognition algorithm were not compared and validated by an independent technique such as SEM-EDS, which makes it difficult to evaluate the utility and the validity of this unsupervised pattern recognition algorithm. Unsupervised machine learning algorithms such as k-means and MCR-ALS can wrongly assign as a single class a mixed mineralogy spectral pattern, which has the effect of misleading the end-user.

Considering the need for fast analysis time and high throughput, LIBS emerges as an ideal sensing technique for mine site applications. Additionally, since the instruments manufactured by EMISSION do not require special devices such as pumps, gases other than air or exhaust fans, they can be used both in the analytical laboratory and in harsh field conditions. A recent study by Rifai et al. using the LIBS CORIOSITY EMISSION technology was carried out on drill core fragments from the PGE Stillwater mine in USA [23]. The main objective of that study was to perform a rapid LIBS surface analysis of a core sample, to assess its mineral content, and to render elemental and mineralogical maps. The mineral phases assignment was made using only the spectra elemental content, and this process was not validated by any other technique. As a result, some mineral phases were not correctly identified, as discussed later in the present manuscript.

In the present manuscript, the LIBS mineral library was built on the basis of the TIMA-X automated mineralogical information. LIBS analyses based on this mineral library were discussed and compared to TIMA-X mineral maps. In addition, the robustness of the supervised machine learning algorithm was verified by predicting the mineralogy of the sample PGE2 (independent test set) from the hyperspectral data obtained during previous work using the same LIBS instrument [23]. Moreover, the quantitative automated mineralogical information obtained by both techniques was compared.

2. Methodology

The principal objective of this study is to demonstrate the new mineral identification functionality of the LIBS technology developed by EMISSION using a supervised method. The PGE-bearing core samples, PGE1a, PGE1b, PGE1c, and PGE2, used for this study are described in Table 1.

Table 1. Geological information on the PGE1 and PGE2 core samples.

PGE1a, b, and c	
Rock type	PGE-bearing ultramafic core samples
Origin	Stillwater complex, USA
Mineral content	Major minerals: bytownite (feldspar), zoisite (epidote), pigeonite (pyroxene), chalcopyrite, pyrite PGE-bearing: pentlandite, pyrrhotite
Analysis method	TIMA-X and LIBS with TIMA validated LIBS mineral library
PGE2	
Rock type	PGE-bearing ultramafic core sample
Origin	Stillwater complex, USA
Mineral content	Same as PGE1 plus presence of PGE-bearing native braggite
Analysis method	Unsupervised LIBS and previous work [23], and TIMA validated LIBS mineral library

Abbreviations: PGE: Platinum-group elements, TIMA: TESCAN Integrated Mineral Analyzer, LIBS: Laser-induced breakdown spectroscopy.

The correspondence between the LIBS spectral fingerprints and the mineral phases was established by means of the PGE1 samples by comparing the TIMA-X image with the LIBS hyperspectral cube (x, y, λ) and by resolving the elementary content of the LIBS spectra. A proprietary supervised machine learning algorithm, implemented in EMISSION software (ELEDIT 2.1.1, OEM LIBS manufacturer,

Montreal, QC, Canada), then processed the training data. The validity of the learning method and of the LIBS analyzes was evaluated by comparison with the TIMA-X mineral map. Since the PGE2 sample (not analyzed by TIMA-X) contains braggite, unlike the PGE1 samples, this mineral was identified by its elemental content only, and it was added to the LIBS mineral library. It is important to note that the LIBS mineral map generated for the PGE2 sample (see Section 3) is based only on training the algorithm using the PGE1 samples. The LIBS analysis was performed using the LIBS CORIOSITY instrument manufactured by ELEMISSION (Figure 1a). The SEM-EDS mineralogical analysis was performed with a TIMA-X instrument (TESCAN, Kohoutovice, Czech Republic) (Figure 1b).



Figure 1. (a) LIBS CORIOSITY mineral analyzer and (b) TIMA-X with a 100-sample autoloader.

2.1. TIMA-X Methodology

2.1.1. Sample Preparation

The three samples PGE1a, b, and c consist of small fragments of drill cores collected in the PGE sulfide mineralized zone of the Stillwater mine (Nye, MT, USA). The samples were provided by First Drilling company (Montrose, CO, USA). Unlike LIBS, TIMA-X requires the sample surface to be perfectly flat for the automated analysis. Sample preparation involves cutting, polishing, and carbon coating the drill core fragments. The drill press Hafco Metalmaster BD-360 was first used to obtain a cylindrical block of 25 mm in diameter, which was then flattened using Secotom-50, a semi-automated cutting tool from Struers. The sample edges were then smoothed with a grinding stone, and the sample surface was polished using LaboForce-100, semi-automated polishing equipment from Struers. A thin layer (20 nm) of carbon was applied on the sample surface using the Q150T ES carbon coater from Quorum. The overall time required to prepare one sample for the TIMA analysis was about 1 h.

The image of the polished block is shown in Figure 2. A bright circle of 19.2 mm in diameter highlights the 289 mm² area scanned by TIMA-X.

2.1.2. TIMA-X Technical Overview

The TIMA instrument that was used for this study is equipped with a field emission gun (FEG), four silicon drift detectors (SDD) from EDAX, and a 100-sample autoloader. A first analysis of the sample was performed by the company AXT of Western Australia using the non-destructive TIMA-X technique.

2.1.3. TIMA-X Procedure

The Dot Mapping mode of TIMA-X measurements was used to perform the automated analysis of rock specimen containing PGEs. The BSE image was first captured at high resolution to detect the boundaries between mineral phases and to locate a central point within each phase. These phases

were then covered by a low-resolution X-ray point mesh for EDS measurements. Areas with similar BSE and EDS values were instantly segmented, and mineral phases were automatically defined based on these signatures. Since PGEs are known to be generally finely disseminated, the Dot Mapping mode was chosen as it is the most suitable for the analysis of fine mineral inclusions. The resolution of the measurement was 3 μm , and the total data acquisition time was approximately 2 h 12 min, excluding the 1 h sample preparation. Table 2 displays the TIMA-X model and parameters used for data acquisition.

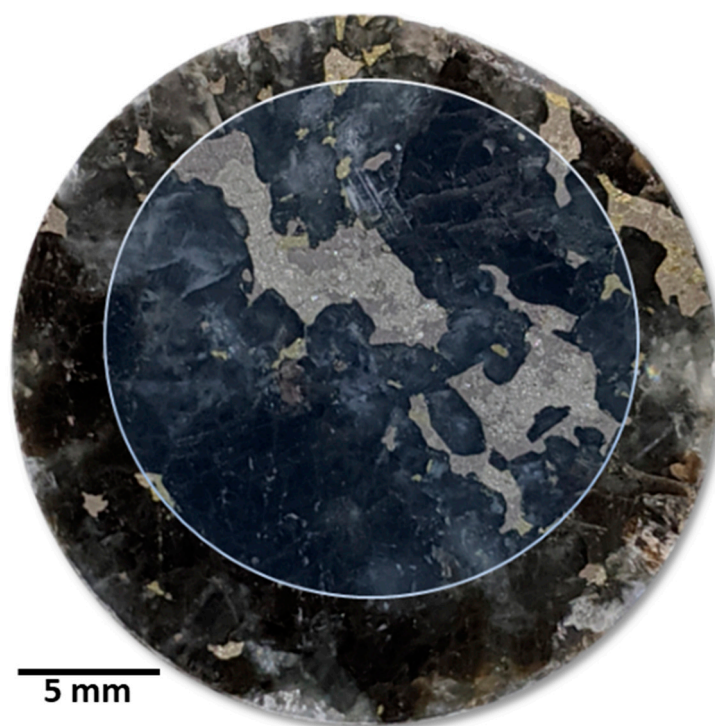


Figure 2. Image of PGE1a polished rock specimen of 25 mm in diameter scanner with TIMA-X (bright circled area of 19.2 mm of diameter) and with LIBS (whole sample).

Table 2. TIMA measurement settings used for the PGE rock specimen analysis.

Electron Beam	
Beam energy	25,000 eV
Probe current	7.21 nA
Beam intensity	18.99
Spot size	62.30 nm
Working distance	15.0 mm
Scanning mode	RESOLUTION
Device	
SEM Type	TIMA3 LMU FEG
Serial number	116-0229
Spectrometer channels	1 + 2 + 3 + 4
Detector model	EDAX Element 30
Calibration set point	420 kcps

Table 2. Cont.

Acquisition	
Acquisition mode	Dot mapping
Pixel spacing	3 μm
Fields scanned	440
Total duration	2 h 12 min
Software version	TESCAN TIMA 1.6.59

2.2. LIBS Methodology

2.2.1. LIBS Technical Overview

In this study, all the LIBS experiments were performed using the LIBS CORIOSITY-G3 analyzer manufactured by ELEMISSION Inc. (Montréal, QC, Canada). The LIBS CORIOSITY analyzer is a fully automated commercial instrument that integrates electronics, the laser source, the spectrometer, and the class one ablation chamber in a single box. This LIBS analyzer is also equipped with an autofocus system to ensure the sample is positioned at the focal plane (minimum spot size) within a range of less than 30 μm from the optimal value. In addition, a high-resolution optical camera gives the end-user a view of the sampling area to optimize the precise positioning of the sample.

The generated plasma emission is collected by achromatic lenses to warrant a minimum chromatic shift over the entire spectrum. The sensitivity of a broad bandpass is consequently enhanced. The optical signal is then spectrally resolved using an optical spectrometer that covers 220 to 930 nm. The spectrometer is equipped with a complementary metal-oxide-semiconductor (CMOS) detector, which is controlled by proprietary electronics. The unique custom electronics allow a camera readout of 1000 full frames per second. The LIBS CORIOSITY analyzer renders 40 \times 40 mm² maximal area scans, but there is room in the ablation chamber to consecutively analyze a bigger sample if required using automated moving linear stage.

2.2.2. Sample Preparation

The LIBS analysis performed with the ELEMISSION's CORIOSITY-G3 instrument did not require sample preparation. Prior to the LIBS analysis, a first cleaning scan was performed to remove the carbon coating applied for the TIMA-X analysis on the surface of the PGE1 samples. This ultra-thin carbon coating, which is required for SEM-EDS measurements, may induce a bias for LIBS measurements by detecting traces of carbon on the sample surface. Even if the PGE-bearing rocks do not contain a lot of carbonates, a laser cleaning step was performed to ensure the accuracy of the measurements. Hence, a cleaning step was performed beforehand to make sure that the LIBS spectra are related only to the minerals naturally present in the rocks.

2.2.3. LIBS Procedure

The LIBS analysis was performed over the whole sample surface illustrated in Figure 2 after the TIMA analysis. Currently, the LIBS analysis can only be performed on a rectangular grid. Considering the cylindrical shape of the polished PGE1 core samples, the latter were put in a polytetrafluoroethylene (PTFE) holder whose hole circumference matched one of the samples. The PTFE holder made it possible to scan the hole area without ablating the CORIOSITY sample holder. Both the rock specimens and the PTFE holder were leveled so that the PTFE did not interfere with the LIBS measurements of the core samples. The total area scanned by LIBS, including the PTFE holder, was 28 \times 28 mm² (about 784 mm²). The scanned area, minus the PTFE holder, was about 491 mm², i.e., the whole 25 mm diameter disk of the PGE1 samples. The PGE2 sample, which had a rectangular shape, was scanned without the need of a PTFE holder. The CORIOSITY parameters for the analysis of the samples PGE1a, b, and c

and PGE2 are detailed in Table 3. As can be seen, the scanning step size for the PGE1 samples was 50 μm , and 100 μm for the PGE2 sample. It is worth mentioning that the predicted relative amounts of minerals using step sizes of 50 and 100 μm were compared on different rocks, but the results are not presented in this manuscript. For major minerals, the predicted percentages were quite similar for both step sizes, while for minor minerals, the predicted percentages for the 100 μm step size were 2–5% lower than those using the 50 μm step size.

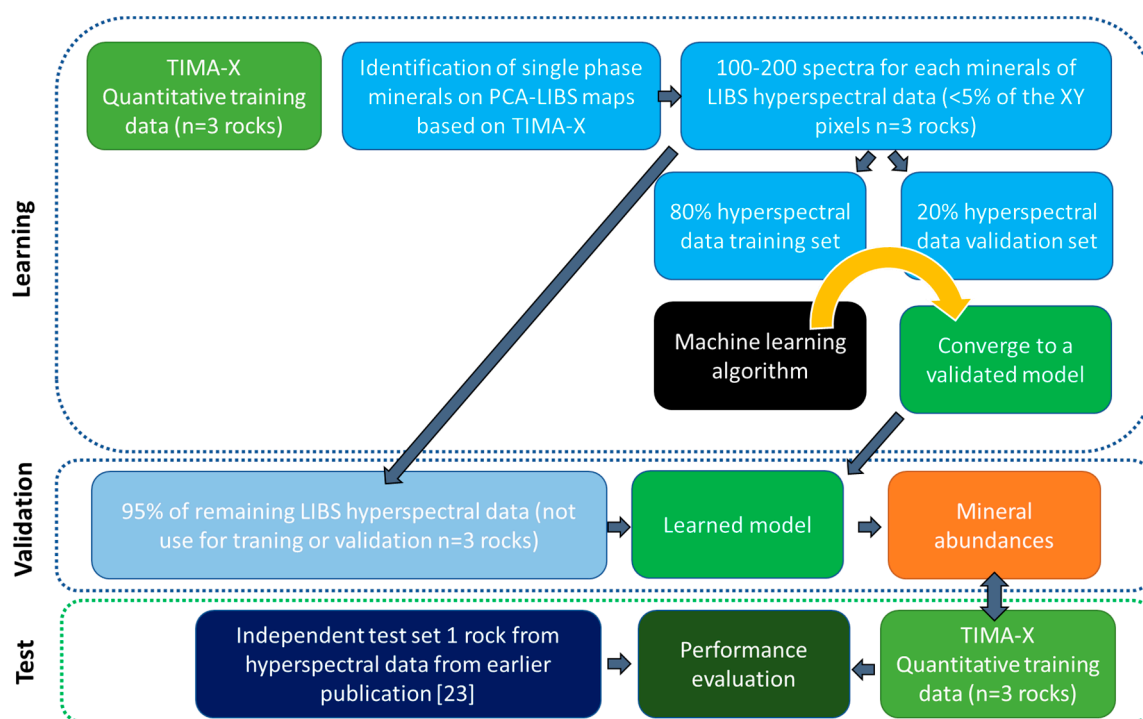
Table 3. Principal LIBS analysis parameters used for the samples PGE1a, b, and c, and PGE2.

LIBS CORIOSITY-G3 Analyzer	
Laser energy	1 mJ/pulse
Laser source wavelength	1064 nm
Acquisition rate	1000 Hz
Spatial resolution	50 μm
Rayleigh zone (depth of field)	5 mm
Working distance (optical window-sample surface)	150 mm
PGE1a, b, and c	
Step size	50 μm
Surface analysed (sample + PTFE holder)	28 \times 28 mm ²
Total duration	5 min 15 s
PGE2 (same sample as in previous work [23])	
Step size	100 μm
Surface analyzed	20 \times 20 mm ²
Total duration	2 min 40 s

To identify mineral phases from LIBS spectra, several strategies are possible. The minerals can be identified from single element maps, or the PCA score map can be interpreted using the typical spectral patterns in the different areas, as done in our previous work [23]. However, implementing a supervised machine learning algorithm is essential for the automatic and reliable identification of minerals.

The ELEdit software integrates the three essential phases of machine learning, which are summarized in Scheme 1. The learning phase begins after the sample area was scanned by the laser. An image based on the first three components of a PCA was generated from the hyperspectral data, as described previously [23]. Identification of the mineral phases of the PGE1 samples was made using the TIMA-X results, the elemental content, and the PCA image. Approximately 100 to 200 spectra, representing less than 5% of the data contained in the hyperspectral data cube, were chosen to describe each single-phase mineral. For each single-phase mineral, 80% of the chosen spectra are put in the training set, and the remaining 20% spectra are put in the validation set. Note that the percentage of spectra used in the training and validation sets can be defined by the software's power-user. The machine algorithm iterates and converges to a validated model that terminates the learning phase. The validation phase is initiated by using external validation data (data that was not used for training or for the cross-validation process, i.e., 95% of the remaining hyperspectral data for PGE1a, b, and c, which represent more than 500,000 spectra). Predicted mineral abundances obtained by LIBS are compared to TIMA-X results for PGE1 samples. Finally, a completely independent test set, which represents an additional good practice in machine learning, was set up by using data taken from a sample analyzed in previous work on PGEs [23], here called the PGE2 sample. It is important to note that this independent test set had several metrics that define such a set: Different days, several months between LIBS measurements of samples PGE2 and PGE1 samples, different experimenters, and exposure of the LIBS instrument to drift (the demonstration unit made 2 international trips between measurements of the PGE2 and PGE1 samples). Good practice

in machine learning suggests having at least one metric, but here we have three metrics that characterize this independent set. The identification of the phases of the PGE2 sample was based on the identified phases of the PGE1 samples and on our previous work [23]. The analysis of the samples PGE1a, b, and c and PGE2 are further discussed in the next section. The software also displays the mineral content using user-defined colors for each identified mineral phase.



Scheme 1. Schematic of the machine learning process automated in EEdit to build the LIBS mineral library: learning phase, validation, and testing.

3. Discussion

3.1. TIMA-X Results

The size of the areas analyzed using the TIMA-X was considerably smaller (1.7 times) than the one analyzed using the LIBS CORIOSITY. The SEM-EDS analyzer has a sample size limit, and the whole surface may not always be scanned. The CORIOSITY G3 can accommodate a drill core fragment up to 35 cm in length; however, the LIBS system dedicated for in-situ analysis can accommodate any size of drill core boxes. As mentioned earlier, the carbon coating required for the TIMA-X analysis was ablated using the LIBS CORIOSITY laser. Although the ablated depth of the cleaned surface was not larger than about 5 μm (much larger than the 20 nm carbon coating), the small layer ablated with the carbon coating can have a possible impact on the computed mineral contents. However, it is important to keep in mind that the LIBS analysis does not systematically require a precleaning step.

In the following, we show the results for the PGE1a sample only. Mineralogical data obtained from TIMA-X (Figure 3) revealed that the main mineral components of the rock sample PGE1a were Ca-rich plagioclase (bytownite) and pyroxene (pigeonite with lamellae of augite exsolution, data not shown). The sample was also particularly rich in coarse-grained pentlandite and pyrrhotite, accompanied by fine chalcopyrite and pyrite. The pentlandite exhibited various concentrations of palladium ranging from 0.01 to 3.5% (1% Pd on average). The remaining PGEs occurred as Pd-Pt tellurides (telluropalladinite, kotulskite, and moncheite), which were finely disseminated in plagioclase, often in close association with pentlandite and chalcopyrite. PGE inclusions were often less than 5 μm in size. A few larger (>20 μm) mineral species containing Pt and Pd (braggite-vysotskite series) were found in the pentlandite.

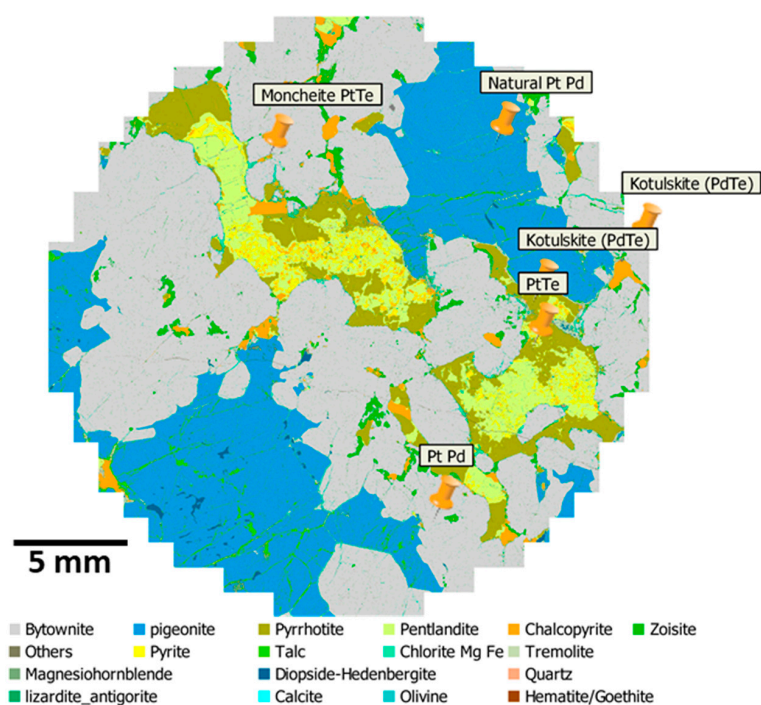


Figure 3. Mineral map obtained by TIMA for the PGE1a sample.

The chemical formula of the most abundant minerals identified from the TIMA-X scan is given in Table 4.

Table 4. Chemical formula of the main mineralogical content observed in the rendered PGE1a TIMA image according to the online Mineral Database [24].

Mineral Phase	Chemical Formula
Bytownite (plagioclase)	$(Ca,Na)(Si,Al)_4O_8$
Pigeonite (pyroxene)	$(Mg,Fe,Ca)(Mg,Fe)Si_2O_6$
Pentlandite (Fe-Ni sulfide)	$(Fe,Ni)_9S_8$
Chalcocopyrite (Cu-Fe sulfide)	$CuFeS_2$
Pyrrhotite (Fe sulfide)	$Fe_{1-x}S_{x=0-0.17}$
Diopside-Hedenbergite (pyroxene)	$CaMgSi_2O_6-CaFeSi_2O_6$
Pyrite (Fe sulfide)	FeS_2
Talc (magnesium silicate clay)	$Mg_3Si_4O_{10}(OH)_2$
Mg-Fe chlorite (phyllosilicate)	$(Mg,Fe)_5Al(Si_3Al)O_{10}(OH)_8$

3.2. Building the LIBS Mineral Library

In order to identify mineral phases using the LIBS CORIOSITY instrument, we first performed an unsupervised PCA, which automatically generated the RGB (Red, Green, Blue) image shown in Figure 4a. The image revealed three main zones represented as grey, cyan, and violet, which, by comparison with Figure 3, were associated with plagioclase, sulfides, and pyroxene, respectively. It should be noted that minerals of similar chemical composition are generally represented with similar RGB combinations in the PCA-score map. To demonstrate the presence of different sulfide minerals in the cyan area, elemental maps of Fe and Ni are presented in Figure 4b,c. As can be observed, the cyan color in Figure 4a was correlated with the highest concentration of iron and nickel in Figure 4b,c. The low iron intensity in Figure 4b (pastel blue) belonged to the pigeonite mineral, whereas the high iron concentration in

Figure 4b (red) corresponded to the pyrrhotite mineral. The high nickel concentration in Figure 4c was assigned to the pentlandite mineral. Figure 4 additionally features the presence of nickel as generally less abundant in the pyrrhotite than in the pentlandite mineral. These mineral identifications were in good agreement with the TIMA-X analysis of Figure 3.

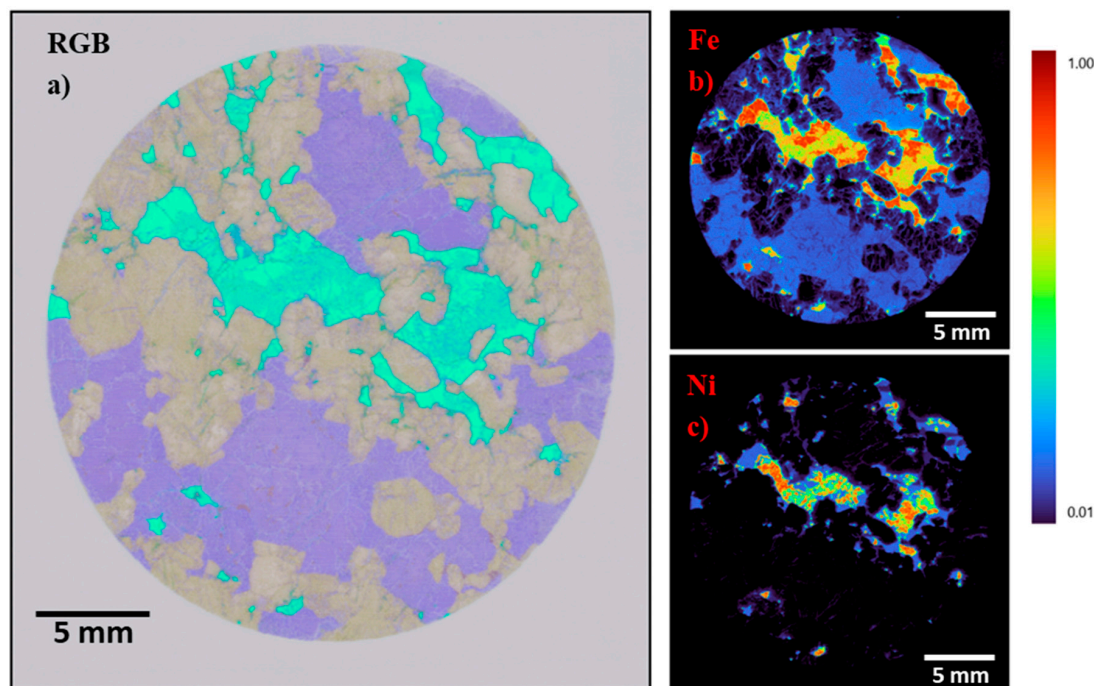


Figure 4. (a) RGB unsupervised PCA LIBS image presenting three major mineral groups (grey: plagioclase, purple: pyroxene, and cyan: sulfides for PGE1a sample); The corresponding elemental heat maps in (b) and (c) highlight the distribution of Fe (sulfides) and Ni (pentlandite), respectively.

Likewise, in the BSE images generated by SEM (data not shown), similar grayscale luminosities were assigned to minerals of the same or similar elemental composition. An important difference between mineral phases assignment using the LIBS PCA pre-imaging and using the SEM BSE pre-imaging is that the PCA is a pre-image of the same identified spectra, while the BSE image has a higher resolution image than the dot mapping EDS data matrix.

3.3. Comparison between TIMA-X and LIBS Results

Single mineral phase assignment is a challenge when comparing a TIMA-X image to lower resolution LIBS hyperspectral matrices because one LIBS spot corresponds to many TIMA-X pixels, and therefore the risk of wrongly identifying a spot containing multiple minerals to a single-phase spot is high. This is why the elemental content has been rigorously analyzed before assigning a LIBS spectrum to a specific mineral phase. Figure 5 shows the spectra ranged between 220–460 nm for the main mineral phases identified by TIMA-X (Figure 3). On the plotted spectra, the main atomic and ionic emission lines were identified. It can be observed that the spectra of the pyrrhotite and the pyrite phases mainly contain iron emission lines. These lines were of higher intensity for the pyrrhotite spectral pattern. The chalcopyrite spectrum was built of iron and copper emission lines, while the pentlandite one was built of iron and nickel lines. The bytownite spectrum was composed mainly of calcium, aluminum, and silicon. The chlorite spectral fingerprint was mainly composed of magnesium, silicon, and aluminum, and a small contribution of iron. In the case of talc, the emission signature mainly displayed magnesium and silicon. The pigeonite spectrum was mainly composed of magnesium, silicon, iron, and a small concentration of calcium and aluminum. Finally, the diopside-hedenbergite spectrum mainly revealed magnesium, calcium, silicon, and iron. It is worth mentioning that there was

a slight discrepancy between the ideal chemical formulas (Table 1) and the multi-elemental composition deduced from the LIBS spectra. After the algorithm assigned a single-phase mineral to each laser shot of the hyperspectral data cube (x, y, λ), a LIBS image could be successfully generated for 13 different minerals. The cases where the laser covers simultaneously mixed mineral phases are discussed below.

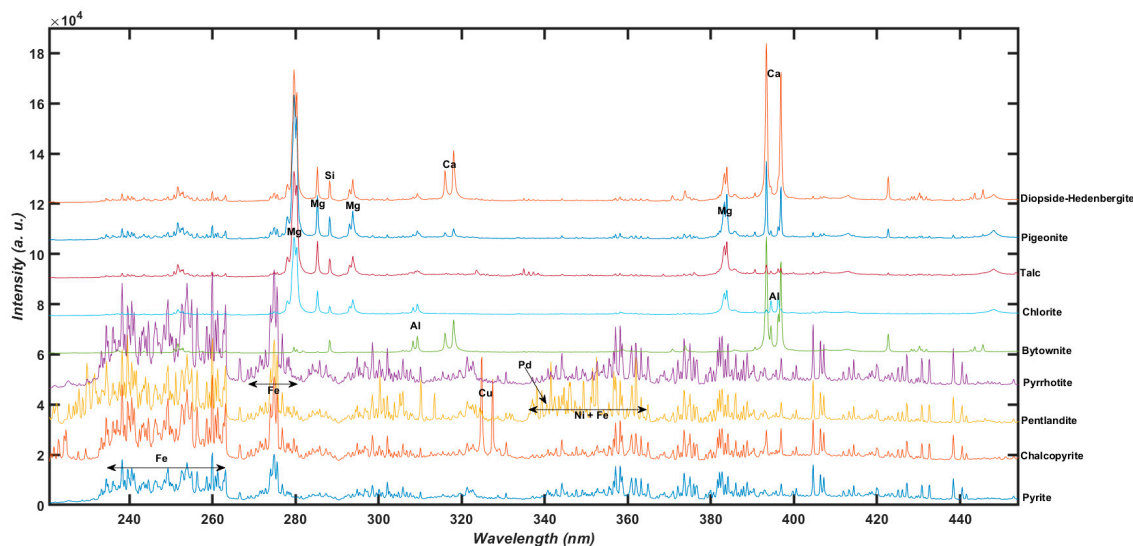


Figure 5. LIBS single-phase spectra of minerals identified from the TIMA-X mineralogical map.

The mineral phase maps illustrated in Figure 6 demonstrated good agreement between the analyses performed with TIMA-X and LIBS CORIOSITY. At first glance, it can be seen that the mapping of the most abundant minerals was similar for both analyses. We see that the small veins of minor minerals were better defined on the mineral map rendered by the TIMA-X due to its higher resolution. For instance, the veins of talc and even the pyrite inclusions were well defined. Furthermore, it was impossible to discern the minor mineral phase of zoisite ($\text{Ca}_2\text{Al}_3(\text{SiO}_4)_3(\text{OH})$) from the major mineral phase of bytownite ($(\text{Ca},\text{Na})(\text{Si},\text{Al})_4\text{O}_8$) in the LIBS CORIOSITY spectral patterns due to their similar elemental content and to the fact that single-phase mineral grains smaller than the spatial resolution of LIBS (i.e., $50 \mu\text{m}$) can hardly be assigned with certitude. Sodium emission lines would improve the assignment process, but at the time the samples were analyzed, the spectral range covered by the LIBS CORIOSITY instrument did not include the strong doublet lines of sodium (589 nm). Since then, the spectral range covered by the instrument has been upgraded by using a new spectrometer, and the discrimination of bytownite and zoisite has become possible (data not shown). The LIBS analysis has not been redone once more with the upgraded instrument because the samples PGE1a, b, and c analyzed by TIMA-X had been ablated by the first LIBS analysis. The mineral content is therefore presented here without distinguishing between bytownite and zoisite.

The few white pixels in the generated LIBS images were pixels that are not assigned to any pure mineral. In such cases, the LIBS spectra collected from these spots had a similarity index of less than 90%, with all spectra corresponding to pure minerals in the mineralogical database. This happens when the laser spot covers a mixed mineral phase, such as at the border of two or more mineral phases or when a minor phase is disseminated into a major one.

To the best of our knowledge, the CORIOSITY instrument is the first and only LIBS instrument capable of discriminating automatically between pyrite and pyrrhotite without requiring an expert in mineralogy to interpret the hyperspectral data. Although, the minerals recognized by LIBS correlated well with those determined by TIMA-X, the mineral mass abundances given in Table 5 showed some differences between the two methods. This is probably due to the fact that the sample area scanned by LIBS was 1.7 times larger than that scanned by TIMA (Figure 2). The area occupied by the minerals, as well as the mineral average density (same for LIBS and TIMA-X), were used to determine the

mass distribution in the TIMA-X and LIBS images. The overall distributions of the main silicates and sulfides have been determined by LIBS with good accuracy, but the analysis of inclusions of fine minerals (calcite, quartz, magnesiohornblende, olivine, and PGEs) presented a larger bias due to the small size of many particles, compared to the diameter of the laser spot. For the PGEs, it is always possible to generate the mono-elemental map, such as presented in Figure 7a, to avoid overwriting the PGE information due to their fine dissemination in other major minerals because of the moderate spatial resolution.

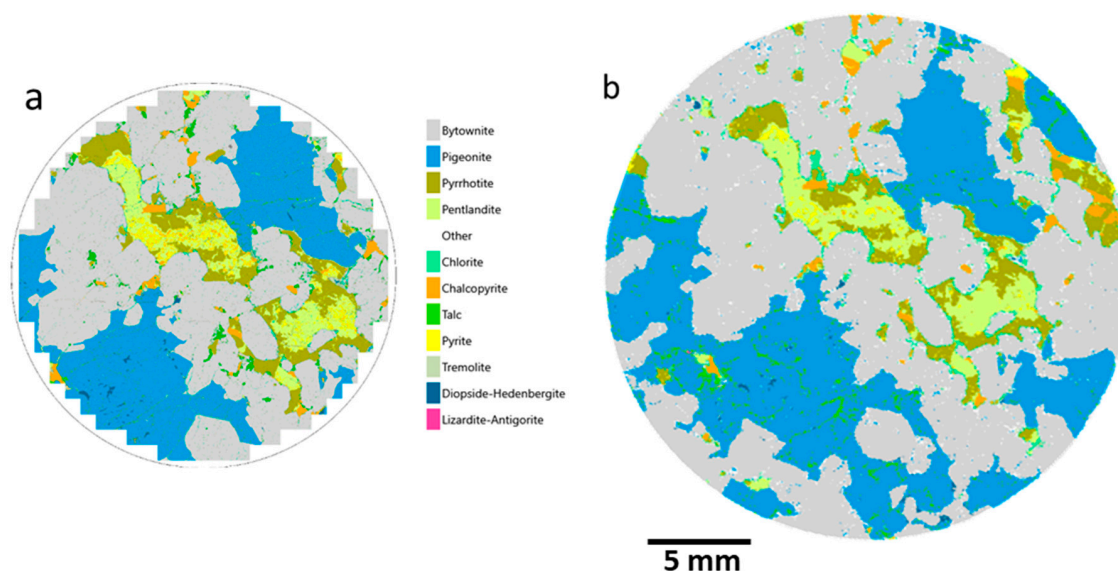


Figure 6. The mineral maps for the PGE1a sample obtained by TIMA (a) and LIBS CORIOSITY (b).

Table 5. The mineral mass distribution obtained by TIMA and LIBS CORIOSITY on PGE1a.

Mineral	TIMA Mineral Mass (%)	LIBS Mineral Mass (%)
Bytownite	41.42	43.06
Pigeonite	26.4	31.57
Pyrrhotite	10.34	7.74
Pentlandite	9.3	7.38
Pyrite	2.36	1.03
Chalcopyrite	2.86	2.11
PGE	0.01	0.01
Chlorite (Mg Fe)	1.03	2.25
Talc	1.06	1.34
Zoisite	2.04	N/D
Diopside-Hedenbergite	0.37	0.36
Tremolite	0.81	0.58
Fe Oxides	0.01	0.01
Lizardite-antigorite	0.04	0.01
Magnesiohornblende	0.37	N/D
Olivine	0.01	N/D
Quartz	0.12	N/D
Calcite	0.02	N/D
Others	1.43	2.86
N/D—not detected		
Total scanned area	289 mm ²	498 mm ²
Measurement resolution	3 μm	50 μm
Total scanning time	2 h 12 min	6 min

Other possible sources of discrepancies between the two methods were differences between the spectral resolution of the two instruments and differences between the depth of the laser ablation and the penetration depth of the electron beam. The cleaning of the carbon coating, as described before, may also have had an impact on the real mineral content since after ablating the surface, the LIBS hyperspectral data represent a mineral distribution somewhat deeper in the rock as compared to the TIMA-X measurements. Yet another factor to consider is the different algorithms used by the two methods to calculate the mineral content.

Going back to the minor minerals found by TIMA-X, such as Pd-Pt tellurides (telluropalladinite, kotulskite, and moncheite), and given that the size of these minerals is less than 5 μm , it was not possible for the LIBS technique to extract pure spectra of those minerals and consequently no pixels were attributed to those minerals in the LIBS images. Nevertheless, it was possible to identify single elements of interest by LIBS, even if they appear as small particles. This is what we illustrate in the following by considering the distribution of palladium. Figure 7a shows the distribution of palladium using its atomic line at 340.45 nm. In Figure 7a, areas containing palladium were encircled and numbered from one to five. These areas correspond to different minerals and different palladium concentrations. The areas one and two represent pentlandite poor (0.01–0.5% *w/w*) and rich (0.5–3.5% *w/w*) in palladium, respectively. The first type of pentlandite is far more abundant than the second type. The areas three to five were assigned to other minerals containing palladium, namely bytownite, pigeonite, and a mix of diopside-hedenbergite and chalcopyrite, respectively. Figure 7b shows the LIBS spectra collected from the five selected areas. Figure 7c is a magnification of Figure 7b. In Figure 7b,c, it can be observed that the spectra of areas one and two corresponded to pentlandite (due to the Ni and Fe lines) with different intensities of the palladium line at 340.45 nm. The palladium lines between 340 and 365 nm exhibited different intensities for different minerals, as can clearly be seen in Figure 7c.

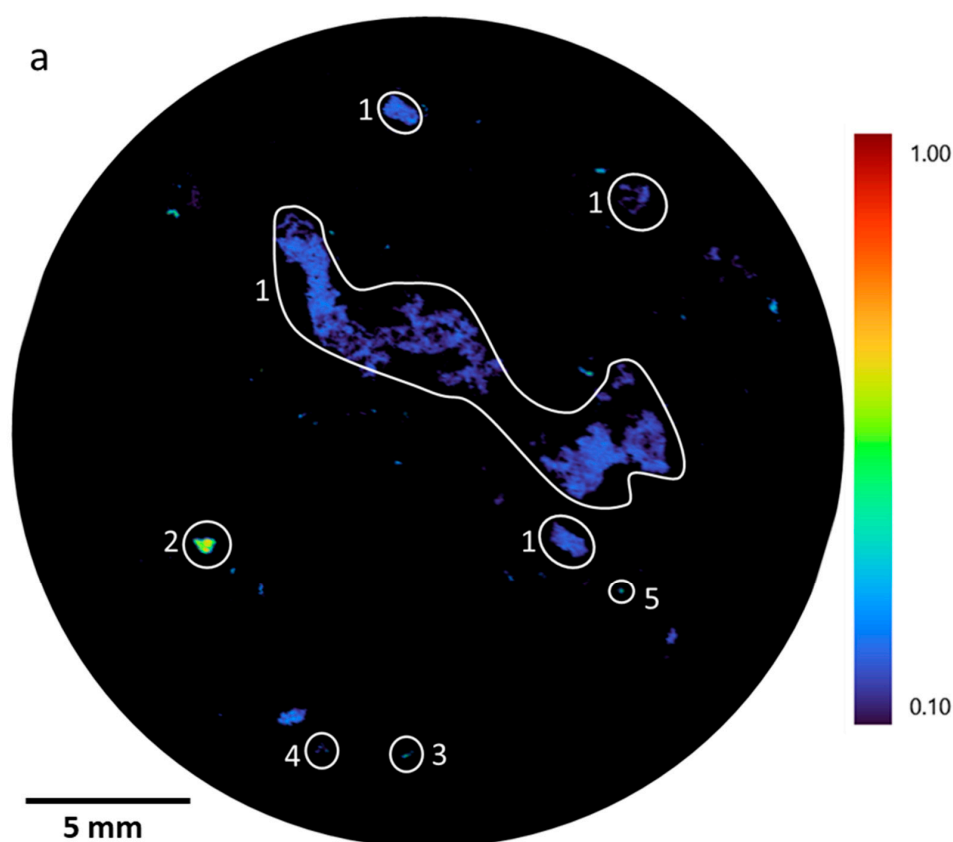


Figure 7. Cont.

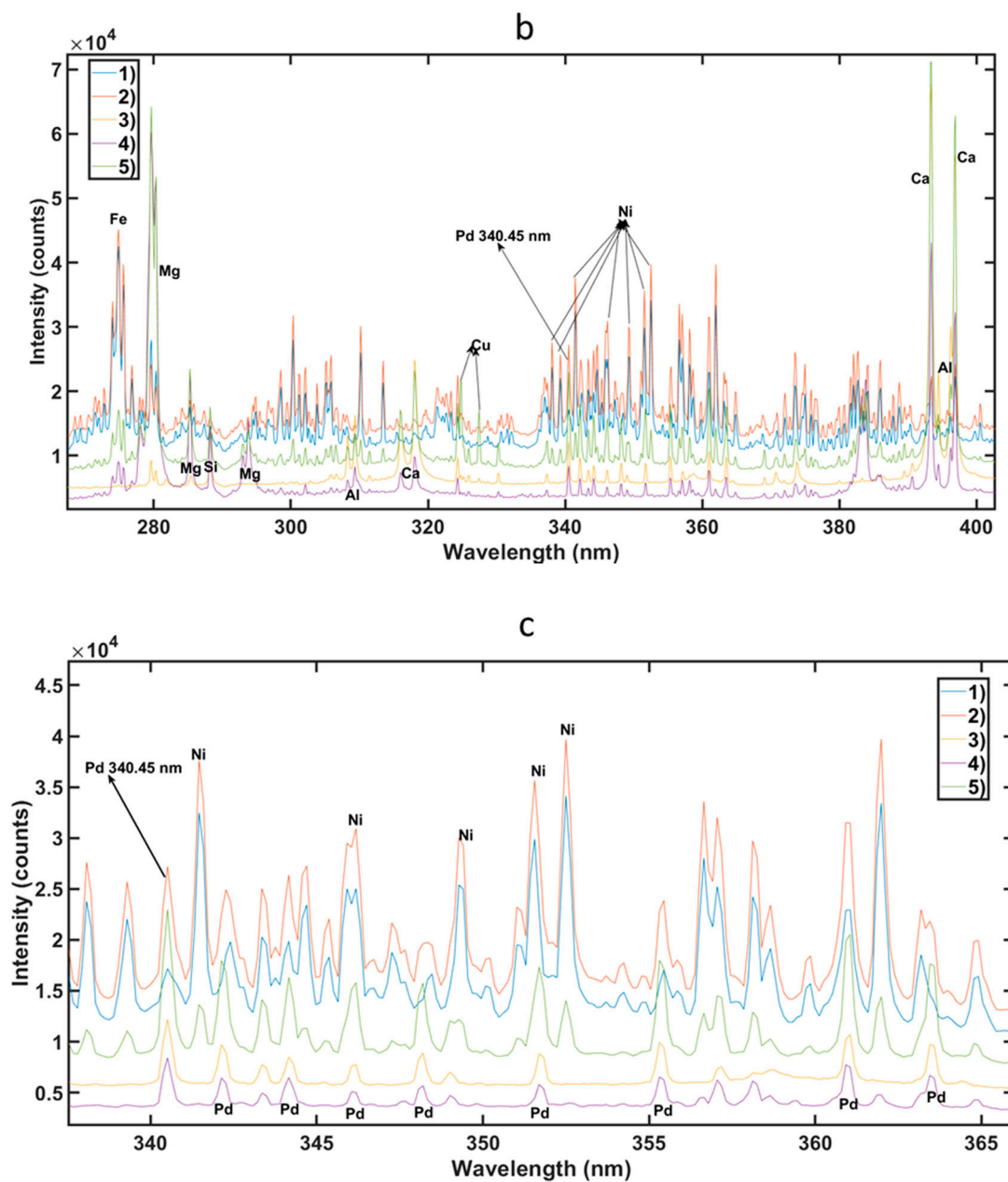


Figure 7. (a) Mono-elemental distribution of palladium determined by LIBS using the Pd I emission line at 340.45 nm; (b) Spectra corresponding to the five encircled areas in Figure 7a; (c) Magnification of the spectra of Figure 7b between 337.5 and 366 nm.

The LIBS mineral library developed from PGE1a, b, and c samples were tested on the PGE2 sample, which was used in a previous study conducted by Rifai et al. [23]. The mineral content determined by LIBS of the sample PGE2, illustrated in Figure 8a–c, shows that it contained relatively coarse grains of PGE-bearing braggite ($>50 \mu\text{m}$), which can be easily analyzed using the LIBS CORIOSITY technology. Prior to conducting the analysis of the mineral content, the braggite phase (not present in the PGE1 samples), identified in [23], was included in the ELeDit mineral library. The minerals maps for PGE1b and PGE1c obtained by TIMA-X and LIBS were in good agreement (data not shown to improve the readability of the manuscript).

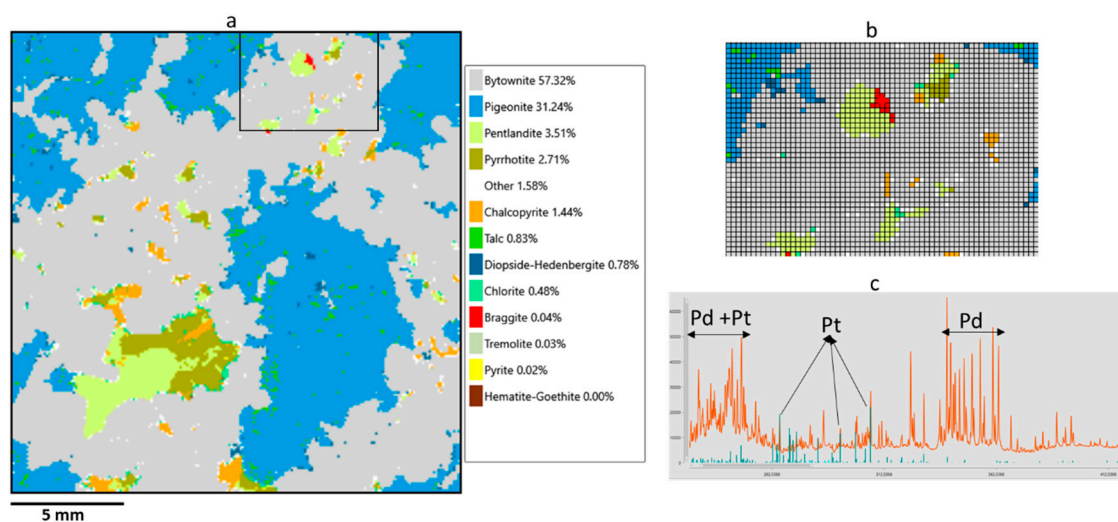


Figure 8. LIBS mineral map of the sample PGE2 used in [23] showing (a) the Pt-Pd mineral braggite (enlarged in (b)) and (c) the braggite spectrum taken in the red area of Figure 8b.

3.4. General Discussion

The LIBS CORIOSITY is a new analysis tool suitable for the ultra-fast quantitative analysis of minerals. Since the LIBS CORIOSITY instrument does not require any special components such as vacuum pumps, gas, or exhaust fans, it can be easily used in the analytical lab as well as in the field.

Combining multiple sensing techniques increases the implementation cost versus efficiency gain ratio. The emergence of the LIBS ultrafast automated quantitative mineral analysis promotes game-changing applications since a single LIBS scan may now render both multielement analysis and quantitative mineralogical analysis, lowering implementation costs and accelerate sample throughput.

The multi-tasks SEM-EDS mapping methods have the majority vote when a high-resolution map has to be generated for geological assessments. Also, EDS spectral databases and mineralogy identification methods are more mature than the LIBS ones because SEM-EDS has been applied to the mining industry for a much longer time. However, it is obvious that the LIBS CORIOSITY is the strongest player from the point of view of the speed of the analyses and transportability. The SEM-EDS method requires a controlled laboratory environment; therefore, the “fieldability” (i.e., the ability of an instrument to be used in any practical field) of SEM-EDS instruments is poor. To countervail some of the technique’s limitations, the TIMA-X was engineered to make the scan speed faster than any other SEM-EDS method. Even with these improvements, the TIMA-X is still considerably slower than the LIBS CORIOSITY instrument. In this study, a larger surface map has been generated using the LIBS instrument in a few minutes, while the TIMA-X mapping took a few hours. The spatial resolution of the LIBS instrument is adapted to field operations; higher resolutions are not needed for in situ mineral liberation analysis. The LIBS technique does not require polishing the sample nor any other preparation step prior to the surface mapping, and it can be applied directly on drill core surfaces without additional cares. On the other hand, SEM-EDS methods require laborious sample preparation. The LIBS multielement and mineralogical analysis is also more sensitive since atomic emission spectra are more complex in the visible spectral range as compared to the X-ray range. The LIBS multi-elemental analysis has no constraints on the atomic weight of chemical elements, contrary to SEM-EDS, which has low sensitivity for elements lighter than magnesium.

From these observations, a radar plot comparing LIBS CORIOSITY versus SEM-EDS is illustrated in Figure 9. From all these practical and scientific considerations, LIBS definitely emerges as a valuable complementary tool for fast, automated mineralogical analysis. In fact, LIBS can help to characterize rapidly rock samples containing high-value minerals that can be characterized afterward using a higher spatial resolution approach such as SEM-EDS. As demonstrated by the implementation of the

extra-terrestrial mining application of the ChemCam instrument on the Mars's Curiosity rover since 2012, LIBS is definitely a valuable tool for surveying the landscape or ore body samples rapidly in order to quickly converge to high-value samples that require deeper investigation with complementary analytical approaches.

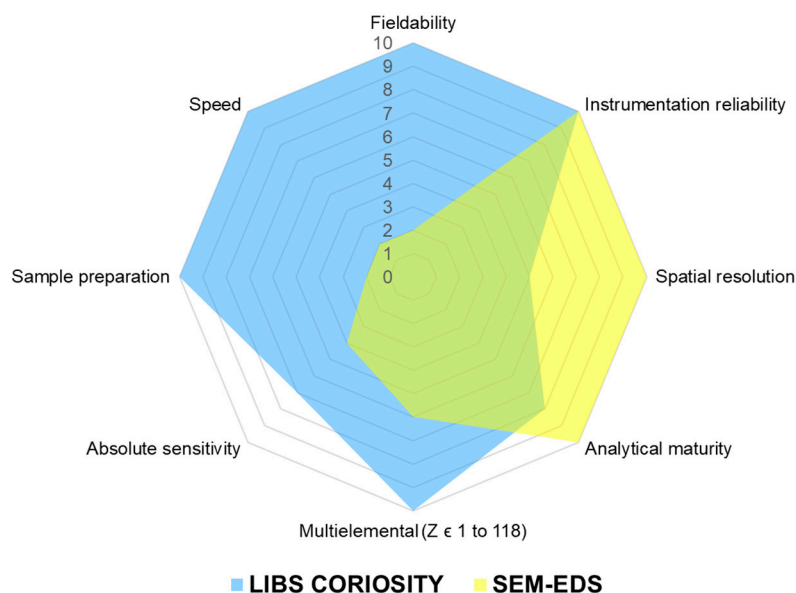


Figure 9. Radar plot of LIBS (blue) and SEM-EDS (yellow) parameters taken in consideration for this study.

4. Conclusions

Mineral surface maps generated using the LIBS technology were compared to TIMA-X maps of the same samples. Similarities between the rendered images and the calculated mineral contents attest to the robustness and quality of the LIBS analysis using the EMISSION CORIOSITY-G3 instrument. The TIMA-X image, elemental content, and PCA image were used to effectively identify single mineral phase spectra from the generated LIBS hyperspectral cube. In addition, it is demonstrated in this study for the first time that it is possible to discriminate different Fe-based mineral phases such as pyrite and pyrrhotite, which has been tried unsuccessfully before by other LIBS researchers [7].

It is also shown in this study that LIBS is a viable fast method that can provide mineralogical content automatically through the development of a LIBS mineral library validated with the state-of-the-art technology TIMA-X. It is clear that the “fieldability” and robustness of LIBS instruments, as demonstrated by the ChemCam on rover Curiosity, make it an unmissable tool to improve and accelerate the discovery of critical elements such as the platinum group elements. The speed and accuracy brought by this new approach have the potential to significantly disrupt the well-established characterization of rock minerals for mining exploration and exploitation. Information such as the mineralogical texture and the pH of the rock has become essential for the future of the mining industry as well as to ensure their completeness in a world with sparser ore deposit. The results obtained in terms of validity, scalability, universality, automation, throughput, and “fieldability” demonstrate that LIBS is the perfect technique for rapidly access the mineralogical information, the multi-elemental content, etc. for characterization of the ore body, for exploration, and exploitation in the mining industry. Although the results presented in this study are very encouraging on small scale rocks; obviously, further works need to be performed to demonstrate the validity of LIBS for PGE as well as other elements on large scale study.

Author Contributions: Conceptualization, K.R., F.D. and L.Ö.; Data curation, K.R. and Z.S.; Formal analysis, K.R., Z.S., A.F. and J.L.; Funding acquisition, F.D. and L.Ö.; Investigation, F.D., L.Ö., A.F. and J.L.; Methodology, K.R., L.Ö. and J.L.; Project administration, F.D., L.Ö. and F.V.; Resources, L.Ö.; Software, F.D.; Supervision, F.D. and L.Ö.; Validation, K.R., Z.S. and J.L.; Writing—original draft, K.R., M.-C.M.P., Z.S. and F.D.; Writing—review & editing, K.R., M.-C.M.P., Z.S., F.D., L.Ö., A.F., J.L. and F.V. All authors have read and agreed to the published version of the manuscript.

Funding: This research was funded by the Mitacs Accelerate program, grant number IT10564, Elemission Inc., and by the National Sciences and Engineering Research Council of Canada.

Acknowledgments: Authors would like to thank Melissa Narbey for contributing to the TIMA experiments, management, and coordination of communication between the different entities.

Conflicts of Interest: The authors declare no conflict of interest.

References

1. Zhang, Z.; Zhao, Z.; Hou, Y.; Wang, H.; Li, X.; He, G.; Zhang, M. Aqueous Platinum(II)—Cage-Based Light-Harvesting System for Photocatalytic Cross-Coupling Hydrogen Evolution Reaction. *Angew. Chem.* **2019**, *131*, 8862–8866. [[CrossRef](#)]
2. Soldevila-Barreda, J.J.; Metzler-Nolte, N. Intracellular Catalysis with Selected Metal Complexes and Metallic Nanoparticles: Advances toward the Development of Catalytic Metallodrugs. *Chem. Rev.* **2019**, *119*, 829–869. [[CrossRef](#)] [[PubMed](#)]
3. Li, G.; Zhao, S.; Zhang, Y.; Tang, Z. Metal-Organic Frameworks Encapsulating Active Nanoparticles as Emerging Composites for Catalysis: Recent Progress and Perspectives. *Adv. Mater.* **2018**, *30*, e1800702. [[CrossRef](#)] [[PubMed](#)]
4. Wu, P.; Wu, Y.; Chen, L.; He, J.; Hua, M.; Zhu, F.; Chu, X.; Xiong, J.; He, M.; Zhu, W.; et al. Boosting aerobic oxidative desulfurization performance in fuel oil via strong metal-edge interactions between Pt and h-BN. *Chem. Eng. J.* **2020**, *380*. [[CrossRef](#)]
5. Amer, M.S.; Ghanem, M.A.; Al-Mayouf, A.M.; Arunachalam, P.; Khadary, N.H. Low-loading of oxidized platinum nanoparticles into mesoporous titanium dioxide for effective and durable hydrogen evolution in acidic media. *Arab. J. Chem.* **2020**, *13*, 2257–2270. [[CrossRef](#)]
6. Oberthür, T. The Fate of Platinum-Group Minerals in the Exogenic Environment—From Sulfide Ores via Oxidized Ores into Placers: Case Studies Bushveld Complex, South Africa, and Great Dyke, Zimbabwe. *Minerals* **2018**, *8*, 581. [[CrossRef](#)]
7. Meima, J.A.; Rammlair, D. Investigation of compositional variations in chromitite ore with imaging Laser Induced Breakdown Spectroscopy and Spectral Angle Mapper classification algorithm. *Chem. Geol.* **2020**, *532*, 119376. [[CrossRef](#)]
8. Gu, Y. Automated Scanning Electron Microscope Based Mineral Liberation Analysis an Introduction to JKMR/FEI Mineral Liberation Analyser. *J. Miner. Mater. Charact. Eng.* **2003**, *2*, 33–41. [[CrossRef](#)]
9. Gottlieb, P.; Wilkie, G.; Sutherland, D.; Ho-Tun, E.; Suthers, S.; Perera, K.; Jenkins, B.; Spencer, S.; Butcher, A.; Rayner, J. Using quantitative electron microscopy for process mineralogy applications. *JOM* **2000**, *52*, 24–25. [[CrossRef](#)]
10. Hrstka, T.; Gottlieb, P.; Skála, R.; Breiter, K.; Motl, D. Automated mineralogy and petrology—Applications of TESCAN Integrated Mineral Analyzer (TIMA). *J. Geosci.* **2018**, *10*, 47–63. [[CrossRef](#)]
11. Honeyands, T.; Manuel, J.; Matthews, L.; O’Dea, D.; Pinson, D.; Leedham, J.; Zhang, G.; Li, H.; Monaghan, B.; Liu, X.; et al. Comparison of the Mineralogy of Iron Ore Sinters Using a Range of Techniques. *Minerals* **2019**, *9*, 333. [[CrossRef](#)]
12. Andersen, A.K.; Zientek, M.L.; Wyss, G. *TIMA-X Bright Phase Analysis of Platinum-Group Minerals in Selected Samples from the Chrome and Iron Mountain Areas of the Stillwater Complex*. Montana; Geological Survey Data Release: Spokane, WA, USA, 2019.
13. Russ, J.C. *Fundamentals of Energy Dispersive X-ray Analysis*; Butterworths: London, UK, 1984.
14. Harmon, R.S.; Russo, R.E.; Hark, R.R. Applications of laser-induced breakdown spectroscopy for geochemical and environmental analysis: A comprehensive review. *Spectrochim. Acta Part B At. Spectrosc.* **2013**, *87*, 11–26. [[CrossRef](#)]

15. Harmon, R.S.; Lawley, C.J.; Watts, J.; Harraden, C.L.; Somers, A.M.; Hark, R.R. Laser-Induced Breakdown Spectroscopy—An Emerging Analytical Tool for Mineral Exploration. *Minerals* **2019**, *9*, 718. [[CrossRef](#)]
16. Jolivet, L.; Leprince, M.; Moncayo, S.; Sorbier, L.; Lienemann, C.-P.; Motto-Ros, V. Review of the recent advances and applications of LIBS-based imaging. *Spectrochim. Acta Part B At. Spectrosc.* **2019**, *151*, 41–53. [[CrossRef](#)]
17. Gottlieb, C.; Millar, S.; Grothe, S.; Wilsch, G. 2D evaluation of spectral LIBS data derived from heterogeneous materials using cluster algorithm. *Spectrochim. Acta Part B At. Spectrosc.* **2017**, *134*, 58–68. [[CrossRef](#)]
18. Romppanen, S.; Häkkinen, H.; Kaski, S. Singular value decomposition approach to the yttrium occurrence in mineral maps of rare earth element ores using laser-induced breakdown spectroscopy. *Spectrochim. Acta Part B At. Spectrosc.* **2017**, *134*, 69–74. [[CrossRef](#)]
19. Pagnotta, S.; Lezzerini, M.; Campanella, B.; Gallelo, G.; Grifoni, E.; Legnaioli, S.; Lorenzetti, G.; Poggialini, F.; Raneri, S.; Safi, A.; et al. Fast quantitative elemental mapping of highly inhomogeneous materials by micro-Laser-Induced Breakdown Spectroscopy. *Spectrochim. Acta Part B At. Spectrosc.* **2018**, *146*, 9–15. [[CrossRef](#)]
20. El Haddad, J.; Filho, E.S.D.L.; Vanier, F.; Harhira, A.; Padioleau, C.; Sabsabi, M.; Wilkie, G.; Blouin, A. Multiphase mineral identification and quantification by laser-induced breakdown spectroscopy. *Miner. Eng.* **2019**, *134*, 281–290. [[CrossRef](#)]
21. Nikonow, W.; Rammlair, D.; Meima, J.A.; Schodlok, M.C. Advanced mineral characterization and petrographic analysis by μ -EDXRF, LIBS, HSI and hyperspectral data merging. *Miner. Pet.* **2019**, *113*, 417–431. [[CrossRef](#)]
22. Nardecchia, A.; Fabre, C.; Cauzid, J.; Pelascini, F.; Motto-Ros, V.; Duponchel, L. Detection of minor compounds in complex mineral samples from millions of spectra: A new data analysis strategy in LIBS imaging. *Anal. Chim. Acta* **2020**, *1114*, 66–73. [[CrossRef](#)]
23. Rifai, K.; Özcan, L.-Ç.; Doucet, F.R.; Rhoderick, K.; Vidal, F. Ultrafast Elemental Mapping of Platinum Group Elements and Mineral Identification in Platinum-Palladium Ore Using Laser Induced Breakdown Spectroscopy. *Minerals* **2020**, *10*, 207. [[CrossRef](#)]
24. Mineral Database. Available online: <http://www.webmineral.com/> (accessed on 3 September 2020).

Publisher’s Note: MDPI stays neutral with regard to jurisdictional claims in published maps and institutional affiliations.



© 2020 by the authors. Licensee MDPI, Basel, Switzerland. This article is an open access article distributed under the terms and conditions of the Creative Commons Attribution (CC BY) license (<http://creativecommons.org/licenses/by/4.0/>).